Contents lists available at ScienceDirect

# Surface Science

journal homepage: www.elsevier.com/locate/susc





# Effect of single atom Platinum (Pt) doping and facet dependent on the electronic structure and light absorption of Lanthanum Titanium Oxide (La<sub>2</sub>Ti<sub>2</sub>O<sub>7</sub>): A Density Functional Theory study

Qingquan Ma<sup>a</sup>, Wen Zhang<sup>a,b,\*</sup>, Joshua Young<sup>b,\*</sup>

- <sup>a</sup> John A. Reif, Jr. Department of Civil and Environmental Engineering, New Jersey Institute of Technology, Newark NJ, 07102, United States
- b Otto H. York Department of Chemical and Materials Engineering, New Jersey Institute of Technology, Newark NJ, 07102, United States

#### ARTICLE INFO

Keywords:
Single atom catalysis (SAC)
Pt
LTO
Facet dependent
Photocatalytic
DET

Bader analysis

#### ABSTRACT

Charge generation and separation are two key processes for semiconductor photocatalysis. Here, we use Pt as a single atom catalyst to systematically examine the facet-dependent electronic band structure and light absorption of the layered perovskite-type wide-gap semiconductor, lanthanum titanium oxide ( $La_2Ti_2O_7$ , LTO) by means of density functional theory simulations. It is found that single Pt atom doping of different LTO surfaces (here, (100), (101) and (001)) can not only create states in the bandgap that would promote the formation of recombination centers, but also shift the optical absorption edge to the visible region. Interestingly, the Pt doping forms a heterojunction, with the valence band maximum consisting of Pt states and the conduction band minimum consisting of LTO states, respectively. To study the facet dependent surface activity, acetic acid ( $CH_3COOH$ ) was used as a model molecule to investigate the adsorption and charge transfer on the (101), (100) and (001) Pt-LTO surface facets. The results show that the (101) facet could enable stronger adsorption of  $CH_3COOH$  by promoting more electron transfer during the interfacial interaction. Our theoretical findings aim to promote the design and optimization of the single atom catalysts (SACs) for photocatalytic applications and other broad catalysis systems.

### 1. Introduction

Approximately 30% of global gross domestic product (GDP) can be ascribed to the catalysis industry, and about 90% of synthetic chemicals are manufactured by catalytic processes [1]. The growing worldwide population and increasing energy consumption per capita bring forth depleting natural resources and increasing environmental pressures. There is an increasing need to design and synthesize catalysts with higher efficiencies for energy production and environmental pollution remediation. Catalyst development is also at the forefront of renewable energy sequestration, storage and utilization [2]. Catalyst innovation also provides solutions to pollutant and greenhouse gas abatement [3].

To increase available active sites and reaction efficiency per unit mass of catalyst material, nanoparticle co-catalysts have been downsized to the atomic scale to achieve so-called single-atom catalysts (SACs). SACs hold a compelling potential in heterogeneous catalysis because of improved atom utilization efficiency, higher reactivity, and improved selectivity for a range of catalytic reactions [4-6]. SACs are

called as such because of the separation of active metals from one another. Compared to conventional nanoparticles in which only surface atoms could be involved in reactions, SACs enable each atom to participate [7-8]. To form a SAC, noble or transition metal atoms possessing high surface energy are atomically dispersed onto high-surface-area support materials (e.g., metal oxide [9], graphene [10], metal carbide [11], zeolites [12] or carbon nitride [13]), which provide high catalyst loading and further prevent individual metal atoms from aggregating [14-15]. The strong metal-support interaction (SMSI) between the dispersed atoms and support materials leads to a dynamic charge transfer and affect catalytic reactions such as CO oxidation [9], hydrogenation reaction [16], water-gas shift [17], synthesis of H<sub>2</sub>O<sub>2</sub> [18], water splitting [19], and photocatalysis [4], [20-21]. The electronic structure within the unsaturated coordination of each single atom is also distinct from its metallic nano-counterparts and has also been revealed to confer unprecedented catalytic enhancement of photocatalytic [22-25], oxygen reduction [12], [25] and electrocatalytic reactions [26-27]. SACs also reduce the loading amounts of

E-mail addresses: wen.zhang@njit.edu (W. Zhang), jyoung@njit.edu (J. Young).

<sup>\*</sup> Corresponding authors.

Q. Ma et al. Surface Science 715 (2022) 121949

noble metals and therefore can alleviate the issues associated with the scarcity and economic cost of implementing them [28].

Knowledge of the interactions between the metal single atoms and support materials and between the catalyst surface and molecules is critical to achieve high-performance catalysts or catalytic processes. The advances in computational tools are steering the development of catalysts from a "blind" trial and error practice into a course of rational design. A large number of theoretical analyses by density functional theory (DFT) have been performed to calculate the feasibility of target chemical reactions and to deepen the understanding of the role of SACs and their supports, as well as their interaction with reactants and products [11], [24] For example, identifying reaction pathways with minimum energy and evaluating charge transfer mechanisms are commonly performed by free-energy diagrams and Bader charge analysis in DFT [27-29]. Recent DFT studies indicate that electronic structures of TiO2 depend on the facet or the specific exposed atomic arrays of catalysts or catalyst support matrixes [30]. Moreover, the metal--support interaction and the electron-transfer process are also facet dependent.

In this study, we investigate the effect of a single atom dopant on the light absorption and charge separation of a wide band-gap semiconductor, lanthanum titanium oxide (La<sub>2</sub>Ti<sub>2</sub>O<sub>7</sub>, LTO). LTO has been extensively studied in recent years because of its unique characteristics, such as its layered perovskite structure and ferroelectric [31], dielectric [32], and photocatalytic or photoelectric properties [33-34]. However, the photoactivity of LTO is largely dependent on its surface atomic structure. Significantly altered adsorption characteristics and redox abilities have been achieved through strategically modulating the exposed facets of LTO [35-37]. More importantly, the facet controllability when synthesizing LTO permits the potential single atom deposition or modification to achieve facet dependent surface-molecule interaction manipulations. To integrate the advantages of both facets and single-atom catalysts, DFT computations were carried out to determine the structural and electronic properties of the different faceted LTO surfaces before and after deposition of single-atom Pt dopants. Furthermore, the changes of light absorbance were determined by calculation of the adsorption coefficients. The interfacial interactions such as molecular adsorption and charge transfer was comparatively studied on different faceted LTO surfaces to highlight the facet-dependent photocatalytic properties of SACs.

## 2. Computational methods

#### 2.1. Density functional theory (DFT) analysis

We employed the Vienna Ab Initio Simulation Package (VASP) to perform the DFT calculations [38-39] and applied the generalized gradient approximation (GGA) using the Perdew-Burke-Ernzerhof (PBE) formulation [40]. The projector augmented wave (PAW) pseudopotentials were used to describe the ionic cores with a plane wave basis set and kinetic energy cutoff of 700 eV to account for the valence electrons [41-42]. Partial occupancies of the Kohn–Sham orbitals were allowed using the Gaussian smearing method and a width of 0.05 eV. The energy was considered self-consistent when the energy change was smaller than  $10^{-6}$  eV. A geometry optimization was considered converged when the force change was smaller than 0.02 eV•Å $^{-1}$ . Grimme's DFT-D3 methodology was used to describe the dispersion interactions [43]. The atomic charges were obtained from Bader's analysis based on the numerical implementation developed by Henkelman et al. [44].

The equilibrium lattice constants of the monoclinic La<sub>2</sub>Ti<sub>2</sub>O<sub>7</sub> unit cell in the monoclinic P2<sub>1</sub>/4 space group were optimized to be a=7.8172 Å, b=5.5975 Å, c=13.2191 Å,  $\alpha$ =90°,  $\beta$ =98.53°, and  $\gamma$ =90°, when using a 2 × 2 × 1 Monkhorst-Pack k-point grid for Brillouin zone sampling. We built a periodic surface with four layers for different facets. The models contain 88 atoms for (100) facets, 132 atoms for (101) facets and 88 atoms for (001) facets. During structural optimizations, the Gamma

point in the Brillouin zone was also used for k-point sampling. Models of three facets are shown in Fig. 1. The optimal plane wave cutoff and k-point grid density were found by continually increasing them until the self-consistent energy changed by less than 1 meV/atom.

### 2.2. Surface energy determination on different facets

Surface energy represents the stability of the surface; a lower value indicates a more stable surface. The surface energies (E) of LTO (001), (100), and (101) facets without and with single-atom Pt were calculated by Eq. (1) and (2) respectively [45]:

$$E = \left(E_{surf} - nE_{bulk}\right)/2A \tag{1}$$

$$E = \left(E_{surf+Pt} - nE_{bulk} - E_{Pt}\right)/2A \tag{2}$$

where  $E_{surf}$  is the total energy of the LTO surfaces (J) of the monoclinic La<sub>2</sub>Ti<sub>2</sub>O<sub>7</sub> unit cell as constructed above,  $E_{bulk}$  is the bulk energy of the unit cell (J),  $E_{Pt}$  is the energy of the Pt single atom (J),  $E_{surf+Pt}$  is the total energy of the Pt-LTO surface (J), A is the surface area of the supercell (m<sup>2</sup>), the coefficient 2 was used since the upper and lower surfaces are both optimized, and n represents the number of unit cells that the surface contains (n=2 in our study). The total energy of the LTO and Pt-LTO surfaces was calculated using the total free energy in the OUT-CAR after optimizations. The major input parameters are detailed in section S1 in the supporting information (SI).

#### 2.3. Assessment of photo-absorbance properties of LTO and Pt-LTO

The optical absorption spectra of different faceted LTO and Pt-LTO (LTO with deposition of a single Pt atom) were calculated by the Fermi golden rule within the dipole approximation from PBE wave functions. Briefly, the real part of the dielectric function ( $\epsilon_1$ ) was obtained by the Kramers-Kronig transformation [46], and the imaginary part of the dielectric function ( $\epsilon_2$ ) due to direct interband transitions was calculated by a summation over empty states [47]. Within VASP, we included an additional 2000 empty conduction band states to ensure convergence as the imaginary part requires a summation over empty states. This complex dielectric constant was used to compute the complex refractive index (N), consisting of the sum of the refractive index (n) and the extinction coefficient (k), via Eq. (4, 5).

$$N = n + ik$$
 (4)

$$\varepsilon = \varepsilon_1 + i\varepsilon_2 = n^2 - k^2 - 2ink \tag{5}$$

Finally, the adsorption coefficient can be determined from k by Eq. (6):

$$\alpha = \frac{4\pi k}{\lambda} \tag{6}$$

#### 2.4. Molecule-catalyst interaction analysis

The surface adsorption energy between model molecules and LTO/Pt-LTO was calculated to assess if the facet-dependence of LTO could exert a pivotal effect on the photocatalytic activity and adsorption. Acetic acid (CH<sub>3</sub>COOH) was selected for this comparative study as the model molecule. We first optimized the molecular structures by putting the CH<sub>3</sub>COOH molecule in a cubic periodic box with a side length of 20 Å and a  $1 \times 1 \times 1$  Monkhorst-Pack k-point grid for Brillouin zone sampling. Then, the relaxed molecule was place on the Pt single atom or bare LTO surface, and after optimization, the obtained energies were recorded. The adsorption energy (E<sub>ads</sub>) of the adsorbate (A) on different surfaces that were defined in Section 2.1 was calculated by Eq. (7):

$$E_{ads} = E_{A/surf} - E_{surf} - E_{A(g)} \tag{7}$$

where  $E_{A/surf}$ ,  $E_{surf}$  and  $E_{A(g)}$  are the energy of A adsorbed on the catalyst

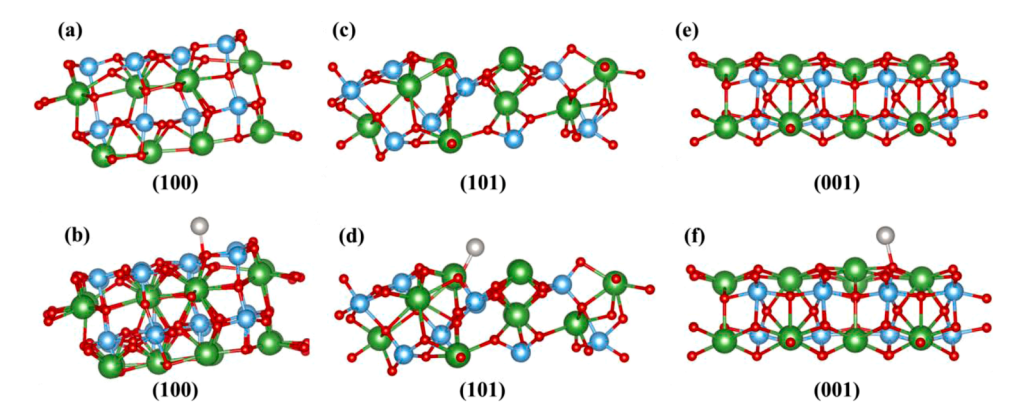


Fig. 1. Schematic of atomic surface structure (a) (100) facet, (c) (101) facet, (e) (001) facet of LTO and (b) (100) facet, (d) (101) facet, (f) (001) facet of Pt-LTO. La, Ti, O, and Pt atoms are illustrated by green, blue, red, and sliver, respectively.

surface (eV), the energy of a clean catalyst surface (eV), and the energy of an isolated A molecule (eV), respectively. Ultimately, the adsorption sites and adsorption mechanisms (e.g., adsorbate-adsorbent configurations and electron transfer) were evaluated by comparing the energies of different adsorption configurations and taking the lowest energy one as the most favorable.

#### 3. Results and discussions

#### 3.1. Pt adsorption configurations and energies

Three different low-index LTO surfaces, (100), (101), and (001), were constructed and are shown in Fig. 1. The surface energies ( $\gamma$ ) of the three different surfaces were calculated with Eq. (1). Through structural optimization of the models, the surface energy of the (100), (101), and (001) facets are 1.20 J•m<sup>-2</sup>, 1.67 J•m<sup>-2</sup> and 0.87 J•m<sup>-2</sup>, respectively. In general, the surface with a higher surface energy has a larger proportion of under-coordinated atoms, which can elicit higher reactivity in heterogeneous reactions [48].

The interaction behavior between Pt and different LTO surface facets was also investigated. To determine the optimal adsorption configuration of Pt on the LTO surfaces, Eads (Eq. (7)) of Pt on each LTO surface for several possible positions of Pt were calculated; the one with the most negative Eads was taken to be the most favorable Pt adsorption site. Fig. S1 in Supporting Information shows examples of these different trial Pt adsorption geometries. The lowest energy optimized structures of the Pt atom on the different LTO surfaces are shown in Fig. 1. For the (100), (101), and (001) facets, the Pt atom is always bonded by one O atom forming a one-coordinated structure with a Pt-O bond length of 1.937, 1.930 and 1.938 Å, respectively. The Pt adsorption energies on the (100), (101), and (001) facets were found to be -2.13, -2.62 and -2.20eV, respectively, indicating that the Pt atom on the (101) LTO surface is stronger compared to the others, in agreement with the surface energy calculations. This strong bonding could also reduce the detachment potential of the single atoms from the catalyst support, which can occur and eventually lead to the loss of photocatalytic activity. Thus, the directed synthesis or growth of the high-energy (101) surface would largely warrant the stable and sufficient loading of the Pt atoms as opposed to the other facets with lower surface energy.

Given that single Pt adsorption can occur and has been investigated on oxide surfaces [49-50] and the strong  $E_{ads}$  of Pt on LTO, the existence of single Pt atoms on this surface is within the realm of possibility. On the other hand, however, individual Pt atoms adsorbed on surfaces are likely to agglomerate into nanoclusters in order to lower the high surface free energy of the single atoms, a well-known phenomenon [51]. As such, we also note that such agglomeration is a distinct possibility here. Unfortunately, within the present means of these calculations, there is no guarantee that this clustering can be avoided and could represent a

significant effect; a more detailed analysis of the single atom and clustering of Pt will be studied in our future work on this system.

#### 3.2. Electronic structure and density of states

DFT calculations were performed to analyze the impact of facets and single Pt atoms on the photocatalytic properties of LTO with exposed (100), (101) and (001) crystal facets. The electronic band gaps ( $E_g$ ) of the different surfaces are determined from the density of states (DOS) as the difference between the valence band maximum (VBM) and conduction band minimum (CBM) and listed in Table 1. First, the electronic density of states (DOS) with the Fermi level set to zero of the (100), (101) and (001) LTO surfaces and that of Pt-LTO surfaces are presented in Fig. 2; from this, we can gain insight into the potential facet dependence of the efficiency of migration and separation of photogenerated electron-hole pairs for LTO. For all the LTO surfaces, the conduction band minima (CBM) consist mainly of Ti d states and a small amount of O p states. The valence band maxima (VBM) are composed predominantly of O p states and a minority of Ti d and La d states. The calculated DOS shows that both VBM and CBM mainly consist of La d, Ti d and O p orbitals, respectively, while contributions from other orbitals are negligible. Moreover, Table 1 shows that the band gaps of the (100), (101) and (001) facets are not equivalent. Zhang et al. reported that specific facets with a smaller band gap have a lower conduction band and a higher valence band, which promotes the generation of electron-hole pairs [52]. Furthermore, the facets that elicit efficient charge separation of electron-hole pairs usually lead to higher photoreactivity [53-54]. In this case, the (101) facet has the narrowest band gap, and as such will likely exhibit higher photoreactivity. Notably, such a prediction of facet dependence was reported previously for the band structure of Cu<sub>2</sub>O [55], TiO<sub>2</sub> [56-57] and LTO [35].

After single Pt atom doping, the top of the conduction band of all three facets moved down significantly as the red arrows indicate in Fig. 2b, d and f. This band shift implies that Pt single atom doping can markedly narrow the band gap of LTO and thus improve its light absorption in the visible-light region. Furthermore, the DOS of Pt-LTO displays an impurity level close to the top of the valence band as indicated by the orange arrows in Fig. 2b, d and f. This impurity state

**Table 1** The calculated relaxed surface energies  $(\gamma)$ , band gaps  $(E_g)$  of different LTO surfaces and Pt adsorption energy  $(E_{ads})$  on LTO surfaces.

LTO/ Pt-LTO Surfaces	γ (J•m <sup>-2</sup> ) (LTO)	γ' (J•m <sup>-2</sup> ) (Pt/ LTO)	$E_g$ (eV)	E <sub>ads</sub> (eV)
(100)	1.20	1.12	1.95	-2.13
(101)	1.67	1.58	1.13	-2.53
(001)	0.87	0.75	2.97	-2.20

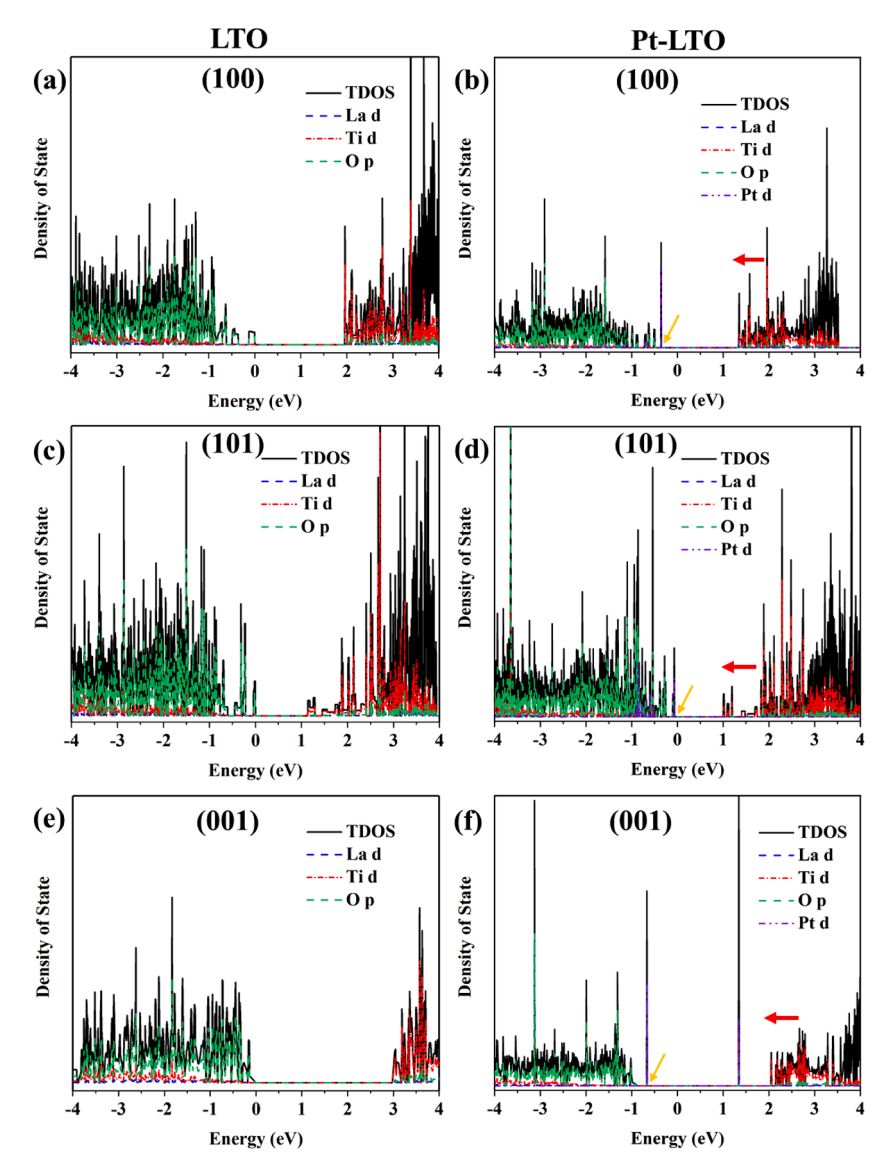


Fig. 2. Density of state (DOS) plots for (a) (100) facet, (c) (101) facets and (e) (001) facets of LTO. (b) (100) facet, (d) (101) facets and (f) (001) facets of Pt-LTO. TDOS, La d, Ti d, O p and Pt d stand for the total density of states and partial density of states of La d, Ti d, O p and Pt d, respectively.

consists of mainly Pt d and O p states, which may extend the light absorption due to the narrowed band gap and enhanced charge transfer. This further explains the common observation of enhanced photocatalytic activity of various photocatalysts (e.g.,  $TiO_2$  [58],  $g-C_3N_4$  [59]

and carbon dots [60]) after Pt doping.

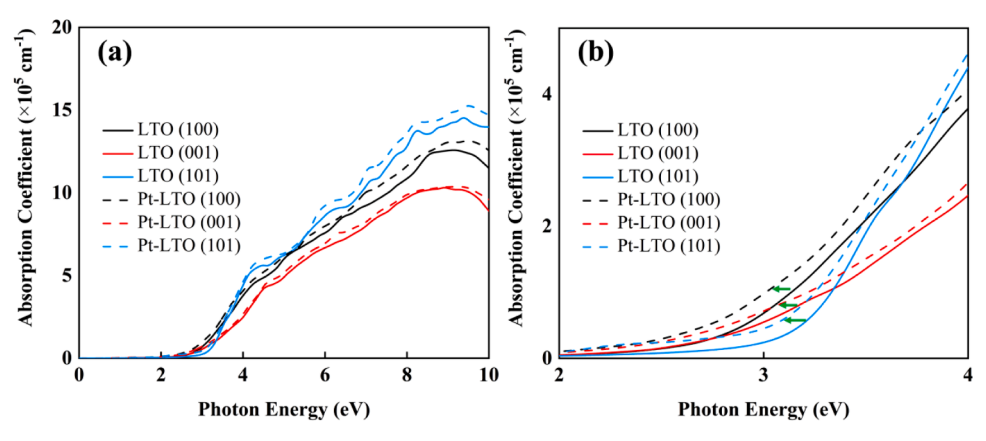


Fig. 3. The direction-averaged optical absorption coefficient spectra for LTO surfaces and Pt-LTO surfaces calculated by the PBEO approach.

Q. Ma et al. Surface Science 715 (2022) 121949

#### 3.3. Comparison of the light absorbance of LTO and Pt-LTO

The key steps in photochemical reactions include light absorption, generation of electron-hole pairs, and transportation of the carriers for participation in photochemical reactions [61]. Among them, the separation efficiency is related to the optical absorption of the semiconductor materials. Therefore, we compared the generation of photogenerated carriers on LTO (100), (101) and (001) facets. Fig. 3a shows that the absorption coefficient of the (101) facet is larger than that of (100) and (001), which is consistent with previous reports [35]. The high absorption coefficient means that the (101) facet could more readily absorb photons, exciting electrons into the conduction band. The impact of the single Pt atom deposition on the absorption coefficients of the three constructed facets is also evident. Fig. 3b shows that the absorption curve shifted to lower energies, as indicated by the green arrows, indicating that Pt doping into different LTO surfaces will extend the light adsorption region due to changes in the band structure. The enhanced light absorption for the Pt doped LTO surfaces are attributed to the offset CBM and the narrowed bandgap relative to the pristine LTO (Fig. 2).

#### 3.4. Bader charge analysis

Bader charge analysis is primarily used for calculating the charge distribution on individual atoms in molecules and crystals. Here, Bader charge analysis was performed to further probe the charge transfer between Pt and LTO and to explain the facet dependent photocatalytic properties of Pt-doped LTO. The electron transfer is driven by the difference between the Fermi energy level of the metal species and the support and is affected by the charge density and distribution of metal species [62]. The charge density difference is defined as the difference between the charge density before and after bonding the corresponding atoms/molecule on the bare surface. Fig. 4a-4c show the charge density difference (CDD) maps of single Pt atoms on the different faceted LTO surfaces generated with an isosurface value of 0.01  $e \cdot \mathring{A}^{-3}$ . The regions of charge depletion and charge accumulation are illustrated by the blue and yellow lobes, respectively. The amounts of electron transfer on different facets are listed in Table 2. The higher amount of electron transfer between the single Pt atom and the LTO surfaces, the stronger the electronic interactions that form, which often lead to greater catalytic activity. Clearly, the (101) facet with single Pt atom modification could result in higher photocatalytic performances than the (100) and (001) facets, as the charge accumulation is nearly double.

## 3.5. The interactions of acetic acid with Pt-LTO

To further probe the differences in these surfaces, the adsorption energies and charge redistribution of acetic acid on each Pt-LTO surfaces were calculated. Acetic acid is one of the most useful model organic pollutants for testing visible-light-driven photocatalysis and is also a simple chemical that contains the full range of C–C, C=O, C–O, O–H, and C–H bonds [63], which allows us to effectively examine these molecular interactions with Pt-LTO. We first constructed various possible adsorption positions of the model molecule on Pt-LTO and bare LTO (100), (101), and (001) surfaces (Fig. S2 and Fig. S3, respectively). The adsorption energy varies with the adsorbate position and orientation on

**Table 2**The charge transfer between single Pt atom and different facets of LTO and Acetic acid and different crystal facets of LTO after absorption.

Facet	Pt on LTO (e)	Acetic acid on Pt-LTO (e)
(100)	-0.14287	0.067142
(101)	-0.34493	-0.54802
(001)	-0.16823	0.040272

the specific surfaces of Pt-LTO. The most stable adsorption configurations and adsorption energies of CH<sub>3</sub>COOH on the three Pt-doped LTO surfaces are presented in Fig. 5. The strongest adsorption energy is obtained when the O of the C=O bond is on the top of the Pt atom, and thus, we selected this configuration to carry out further calculations of the adsorption energy. The E<sub>ads</sub> of acetic acid is similar on the (100) and (001) facets (-1.54 eV and -1.61 eV, respectively). However, the adsorption energy increases dramatically for acetic acid on the Pt-LTO (101) surface (-3.45 eV), as expected from the previous discussion, and thus this surface could more easily facilitate further charge transfer and catalytic reactions. Finally, the E<sub>ads</sub> of acetic acid is significantly lower on the bare LTO surfaces, with values of -0.69, -1.04 and -0.19 eV for (100), (101) and (001), respectively.

The three-dimensional (3D) CDD maps of the CH<sub>3</sub>COOH on the different faceted Pt-LTO surface were built using the VESTA software with an isosurface value of 0.1  $e \cdot A^{-3}$ . Fig. S4 shows the positions of La, Ti, Pt, C, and O atoms and the corresponding electron clouds around them. To understand the bonding nature and charge distribution between CH<sub>3</sub>COOH and Pt-LTO surfaces, the two-dimensional (2D) CDD maps (Fig. 6) of the three different faceted Pt-LTO surfaces are plotted in the range of 0 to 0.2  $e \cdot A^{-3}$  underneath the 3D maps. The red and blue regions correspond to higher and lower charge density region, respectively. Clearly, the electron density of CH<sub>3</sub>COOH on Pt-LTO (101) surface are higher that on (100) and (001) surfaces, implying the electron transfer is different when CH3COOH interacts with different Pt-LTO surfaces. This charge transfer observation agrees with the Bader charge calculation (Table 2), which reveals that the CH<sub>3</sub>COOH molecule on Pt-LTO (101) surfaces gains a net negative charge of 0.54e during adsorption and that more charge is transferred than on the other two facets.

#### 4. Conclusion

In this work, we have investigated single Pt atom doping on three different LTO surfaces ((100), (101) and (001)) using DFT calculations. The results revealed that doping single Pt atoms into three LTO surfaces can narrow the band gap of these LTO surfaces and thus improve its light absorption in the visible-light region. After single atom doping, Pt atoms tend to act as bridges to facilitate the interlayer charge carrier transfer. In particular, the Pt-LTO (101) surface has the narrowest bandgap, implying the most effective charge transfer and the highest optical absorption compared to Pt-LTO (100) and Pt-LTO (001). Moreover, the adsorption of the model pollutant CH<sub>3</sub>COOH on Pt-LTO surfaces also indicates that the Pt-LTO (101) has the most favorable interfacial interaction. Our results are conducive to comprehending the interactive relationship between single-atom noble metal and LTO surfaces and to

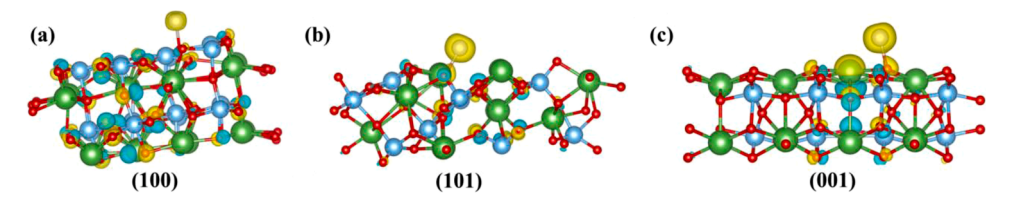


Fig. 4. Three-dimensional charge density difference maps of single Pt atom adsorption on LTO (100) facet (a), (101) facet (b), and (001) facet. O, La, Ti, and Pt atoms are illustrated by red, green, blue, and sliver, respectively.

Fig. 5. Schematic of atomic surface structure (100) facet, (101) facet, (001) facet of acetic acid or PFOA adsorption on Pt-LTO. La, Ti, O, C, H and Pt atoms are illustrated by green, blue, red, brown, pink and sliver, respectively.

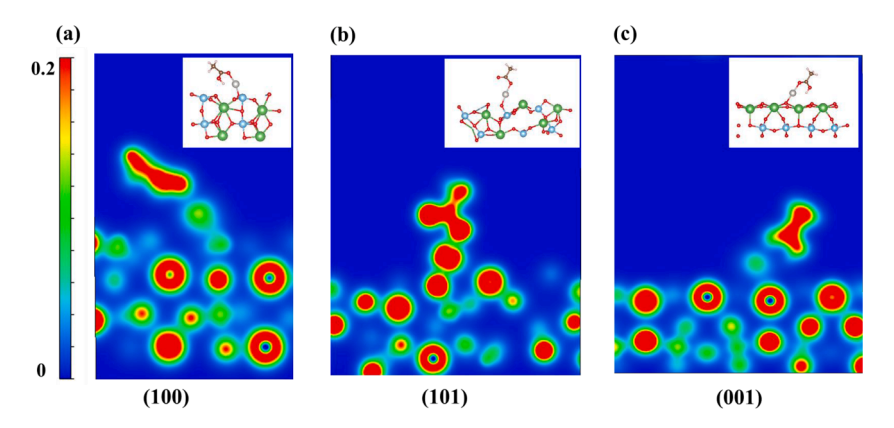


Fig. 6. Two-dimensional charge density distribution and corresponding atomic positions of CH<sub>3</sub>COOH on the different faceted Pt-LTO surfaces.

the design of high-efficiency photocatalyst.

#### CRediT authorship contribution statement

**Qingquan Ma:** Investigation, Formal analysis, Writing – original draft, Visualization. **Wen Zhang:** Conceptualization, Supervision, Writing – review & editing. **Joshua Young:** Supervision, Project administration, Writing – review & editing.

## **Declaration of Competing Interest**

The authors declare that they have no conflict of Interest.

## Acknowledgements

This work was supported by the New Jersey Water Research Resources Institute (NJWRRI) under award number G16AP00071, as well as with startup funds from the Newark College of Engineering at the New Jersey Institute of Technology. DFT calculations were performed on the Kong and Lochness clusters at the New Jersey Institute of Technology, the Extreme Science and Engineering Discovery Environment (XSEDE, supported by NSF Grant No. ACI-1053575) under allocation TG-DMR180009, and the CARBON cluster at the Center for Nanoscale Materials (Argonne National Laboratory, supported by the U.S. DOE, Office of Basic Energy Sciences (BES), DE-AC02–06CH11357) under allocation CNM72868. The faceted nanomaterial synthesis and analysis was also supported by the US National Science Foundation (Award#: 1756444).

#### Supplementary materials

Supplementary material associated with this article can be found, in the online version, at doi:10.1016/j.susc.2021.121949.

#### References

- G.J. Hutchings, M.G. Davidson, R.C. Catlow, C. Hardacre, N.J. Turner, P. Collier, Modern Developments in Catalysis, World Scientific, 2016.
- [2] F.A. Rahman, M.M.A. Aziz, R. Saidur, W.A.W.A. Bakar, M. Hainin, R. Putrajaya, N. A. Hassan, Pollution to solution: capture and sequestration of carbon dioxide (CO2) and its utilization as a renewable energy source for a sustainable future, Renewable Sustainable Energy Rev. 71 (2017) 112–126.
- [3] K. Stangeland, D. Kalai, H. Li, Z. Yu, CO2 methanation: the effect of catalysts and reaction conditions, Energy Procedia 105 (2017) 2022–2027.
- [4] L. Liu, A. Corma, Metal catalysts for heterogeneous catalysis: from single atoms to nanoclusters and nanoparticles, Chem. Rev. 118 (2018) 4981–5079.
- [5] A. Wang, J. Li, T. Zhang, Heterogeneous single-atom catalysis, Nature Rev. Chem. 2 (2018) 65–81.
- [6] H. Zhang, G. Liu, L. Shi, J. Ye, Single-atom catalysts: emerging multifunctional materials in heterogeneous catalysis, Adv. Energy Mater. 8 (2018), 1701343.
- [7] B.-H. Lee, S. Park, M. Kim, A.K. Sinha, S.C. Lee, E. Jung, W.J. Chang, K.-S. Lee, J. H. Kim, S.-P. Cho, Reversible and cooperative photoactivation of single-atom Cu/ TiO 2 photocatalysts, Nature Mater. 18 (2019) 620–626.
- [8] C. Zhu, Q. Shi, S. Feng, D. Du, Y. Lin, Single-atom catalysts for electrochemical water splitting, ACS Energy Lett. 3 (2018) 1713–1721.
- [9] L. Nie, D. Mei, H. Xiong, B. Peng, Z. Ren, X.I.P. Hernandez, A. DeLaRiva, M. Wang, M.H. Engelhard, L. Kovarik, Activation of surface lattice oxygen in single-atom Pt/ CeO2 for low-temperature CO oxidation, ScienceScience 358 (2017) 1419–1423.
- [10] Y. Wang, W. Zhang, D. Deng, X. Bao, Two-dimensional materials confining single atoms for catalysis, Chin. J. Catal. 38 (2017) 1443.
- [11] S. Yang, Y.J. Tak, J. Kim, A. Soon, H. Lee, Support effects in single-atom platinum catalysts for electrochemical oxygen reduction, ACS Catal. 7 (2017) 1301–1307.
- [12] L. Liu, U. Diaz, R. Arenal, G. Agostini, P. Concepción, A. Corma, Generation of subnanometric platinum with high stability during transformation of a 2D zeolite into 3D, Nature Mater. 16 (2017) 132–138.
- [13] Z. Zeng, Y. Su, X. Quan, W. Choi, G. Zhang, N. Liu, B. Kim, S. Chen, H. Yu, S. Zhang, Single-atom platinum confined by the interlayer nanospace of carbon nitride for efficient photocatalytic hydrogen evolution, Nano Energy 69 (2020), 104409.
- [14] S. Mitchell, E. Vorobyeva, J. Pérez-Ramírez, The multifaceted reactivity of singleatom heterogeneous catalysts, Angew. Chem. Int. Ed. 57 (2018) 15316–15329.
- [15] P. Hu, Z. Huang, Z. Amghouz, M. Makkee, F. Xu, F. Kapteijn, A. Dikhtiarenko, Y. Chen, X. Gu, X. Tang, Electronic metal–support interactions in single-atom catalysts, Angew. Chem. 126 (2014) 3486–3489.
- [16] Y. Peng, Z. Geng, S. Zhao, L. Wang, H. Li, X. Wang, X. Zheng, J. Zhu, Z. Li, R. Si, Pt single atoms embedded in the surface of Ni nanocrystals as highly active catalysts for selective hydrogenation of nitro compounds, Nano Lett. 18 (2018) 3785–3791.
- [17] N. Cheng, S. Stambula, D. Wang, M.N. Banis, J. Liu, A. Riese, B. Xiao, R. Li, T.-. K. Sham, L.-.M. Liu, Platinum single-atom and cluster catalysis of the hydrogen evolution reaction, Nat. Commun. 7 (2016) 1–9.

- [18] C.H. Choi, M. Kim, H.C. Kwon, S.J. Cho, S. Yun, H.-T. Kim, K.J. Mayrhofer, H. Kim, M. Choi, Tuning selectivity of electrochemical reactions by atomically dispersed platinum catalyst, Nat. Commun. 7 (2016) 1–9.
- [19] X.P. Yin, H.J. Wang, S.F. Tang, X.L. Lu, M. Shu, R. Si, T.B. Lu, Engineering the coordination environment of single-atom platinum anchored on graphdiyne for optimizing electrocatalytic hydrogen evolution, Angew. Chem. Int. Ed. 57 (2018) 0322, 0326.
- [20] Y. Cao, D. Wang, Y. Lin, W. Liu, L. Cao, X. Liu, W. Zhang, X. Mou, S. Fang, X. Shen, Single Pt atom with highly vacant d-orbital for accelerating photocatalytic H2 evolution, ACS Appl. Energy Mater. 1 (2018) 6082–6088.
- [21] N. Daelman, M. Capdevila-Cortada, N. López, Dynamic charge and oxidation state of Pt/CeO2 single-atom catalysts, Nat. Mater 18 (2019) 1215–1221.
- [22] M. Murdoch, G. Waterhouse, M. Nadeem, J. Metson, M. Keane, R. Howe, J. Llorca, H. Idriss, The effect of gold loading and particle size on photocatalytic hydrogen production from ethanol over Au/TiO 2 nanoparticles, Nat. Chem. 3 (2011) 489–492.
- [23] J. Wang, H. Tan, S. Yu, K. Zhou, Morphological effects of gold clusters on the reactivity of ceria surface oxygen, ACS Catal. 5 (2015) 2873–2881.
- [24] L. Qin, Y.Q. Cui, T.L. Deng, F.H. Wei, X.F. Zhang, Highly stable and active Cu1/ CeO2 single-atom catalyst for CO oxidation: a DFT study, ChemPhysChem 19 (2018) 3346–3349.
- [25] S. Proch, M. Wirth, H.S. White, S.L. Anderson, Strong effects of cluster size and air exposure on oxygen reduction and carbon oxidation electrocatalysis by sizeselected Pt n (n≤ 11) on glassy carbon electrodes, J. Am. Chem. Soc. 135 (2013) 3073–3086
- [26] Z. Li, S. Ji, Y. Liu, X. Cao, S. Tian, Y. Chen, Z. Niu, Y. Li, Well-defined materials for heterogeneous catalysis: from nanoparticles to isolated single-atom sites, Chem. Rev. 120 (2019) 623–682.
- [27] B. Qiao, A. Wang, X. Yang, L.F. Allard, Z. Jiang, Y. Cui, J. Liu, J. Li, T. Zhang, Single-atom catalysis of CO oxidation using Pt 1/FeO x, Nat Chem 3 (2011) 634–641.
- [28] S. Weon, D. Huang, K. Rigby, C. Chu, X. Wu, J.-.H. Kim, Environmental materials beyond and below the nanoscale: single-atom catalysts. ACS ES&T Eng. (2020).
- [29] B. Qiao, J.-.X. Liang, A. Wang, C.-.Q. Xu, J. Li, T. Zhang, J.J. Liu, Ultrastable singleatom gold catalysts with strong covalent metal-support interaction (CMSI), Nano Res. 8 (2015) 2913–2924.
- [30] J. Yu, J. Low, W. Xiao, P. Zhou, M. Jaroniec, Enhanced photocatalytic CO2reduction activity of anatase TiO2 by coexposed {001} and {101} facets, J. Am. Chem. Soc. 136 (2014) 8839–8842.
- [31] H. Yan, H. Ning, Y. Kan, P. Wang, M.J. Reece, Piezoelectric ceramics with superhigh curie points, J. Am. Ceram. Soc. 92 (2009) 2270–2275.
- [32] Y. Lu, C. Le Paven, H.V. Nguyen, R. Benzerga, L. Le Gendre, S. Rioual, F. Tessier, F. Cheviré, A. Sharaiha, C. Delaveaud, Reactive sputtering deposition of perovskite oxide and oxynitride lanthanum titanium films: structural and dielectric characterization. Cryst. Growth Des. 13 (2013) 4852–4858.
- [33] J. Kim, D.W. Hwang, H.-.G. Kim, S.W. Bae, S.M. Ji, J.S. Lee, Nickel-loaded La 2 Ti 2 O 7 as a bifunctional photocatalyst, Chem. Commun. (2002) 2488–2489.
- [34] Z. Wang, K. Teramura, S. Hosokawa, T. Tanaka, Photocatalytic conversion of CO2 in water over Ag-modified La2Ti2O7, Appl. Catal. B 163 (2015) 241–247.
  [35] Z. Huang, J. Liu, L. Huang, L. Tian, S. Wang, G. Zhang, J. Li, F. Liang, H. Zhang,
- [35] Z. Huang, J. Liu, L. Huang, L. Tian, S. Wang, G. Zhang, J. Li, F. Liang, H. Zhang, Q. Jia, One-step synthesis of dandelion-like lanthanum titanate nanostructures for enhanced photocatalytic performance, NPG Asia Mater. 12 (2020) 1–12.
- [36] X. Cai, L. Mao, J. Zhang, M. Zhu, M. Fujitsuka, T. Majima, Charge separation in a nanostep structured perovskite-type photocatalyst induced by successive surface heterojunctions, J. Mater. Chem. A 5 (2017) 10442–10449.
- [37] X. Cai, M. Zhu, O.A. Elbanna, M. Fujitsuka, S. Kim, L. Mao, J. Zhang, T. Majima, Au nanorod photosensitized La2Ti2O7 nanosteps: successive surface heterojunctions boosting visible to near-infrared photocatalytic H2 evolution, ACS Catal. 8 (2018) 122–131.
- [38] G. Kresse, J. Furthmüller, Efficiency of ab-initio total energy calculations for metals and semiconductors using a plane-wave basis set, Comp.mater. 6 (1996) 15–50.
- [39] G. Kresse, F. J. Efficient iterative schemes for ab initio total-energy calculations using a plane-wave basis set, Phys. Rev. B (Condensed Matter) 54 (1996) 11169–11186.

- [40] J.P. Perdew, K. Burke, M. Ernzerhof, Erratum, Generalized Gradient Approximation Made Simple, Phys. Rev. Lett. (1996).
- [41] G. Kresse, D. Joubert, From ultrasoft pseudopotentials to the projector augmentedwave method, Phys. Rev. B 59 (1999) 1758–1775.
- [42] P.E. Blochl, Projector augmented-wave method, Phys. Rev. B Condens Matter 50 (1994) 17953–17979.
- [43] S. Grimme, J. Antony, S. Ehrlich, H. Krieg, A consistent and accurate ab initio parametrization of density functional dispersion correction (DFT-D) for the 94 elements H-Pu, J. Chem. Phys. 132 (2010), 154104.
- [44] G. Henkelman, A. Arnaldsson, H. Jónsson, A fast and robust algorithm for Bader decomposition of charge density, Comput. Mater. Sci. 36 (2006) 354–360.
- [45] L. Zhou, F. Xiu, M. Qiu, S. Xia, L. Yu, The adsorption and dissociation of water molecule on goethite (010) surface: a DFT approach, Appl. Surf. Sci. 392 (2017) 760–767.
- [46] M. Gajdoš, K. Hummer, G. Kresse, J. Furthmüller, F. Bechstedt, Linear optical properties in the projector-augmented wave methodology, Phys. Rev. B 73 (2006), 045112.
- [47] A. Read, R. Needs, Calculation of optical matrix elements with nonlocal pseudopotentials, Phys. Rev. B 44 (1991) 13071.
- [48] S. Rong, P. Zhang, F. Liu, Y. Yang, Engineering crystal facet of α-MnO2 nanowire for highly efficient catalytic oxidation of carcinogenic airborne formaldehyde, ACS Catal. 8 (2018) 3435–3446.
- [49] Q. Wan, V. Fung, S. Lin, Z. Wu, D.-e. Jiang, Perovskite-supported Pt single atoms for methane activation, J. Mater. Chem. A 8 (2020) 4362–4368.
- [50] N. Daelman, M. Capdevila-Cortada, N. López, Dynamic charge and oxidation state of Pt/CeO 2 single-atom catalysts, Nature Mater. 18 (2019) 1215–1221.
- [51] X.-.F. Yang, A. Wang, B. Qiao, J. Li, J. Liu, T. Zhang, Single-atom catalysts: a new frontier in heterogeneous catalysis, Acc. Chem. Res. 46 (2013) 1740–1748.
- [52] H. Zhang, Y. Yang, Z. Zhou, Y. Zhao, L. Liu, Enhanced photocatalytic properties in BiOBr nanosheets with dominantly exposed (102) facets, The J. Phys. Chem. C 118 (2014) 14662–14669.
- [53] J. Li, Y. Sun, G. Jiang, Y. Chu, S. Lee, F. Dong, Tailoring the rate-determining step in photocatalysis via localized excess electrons for efficient and safe air cleaning, Appl. Catal. B 239 (2018) 187–195.
- [54] J. Li, Y. Sun, W. Cen, F. Dong, Facet-dependent interfacial charge separation and transfer in plasmonic photocatalysts, Appl. Catal. B 226 (2018) 269–277.
- [55] M.H. Huang, Facet-Dependent Optical Properties of Semiconductor Nanocrystals, Small 15 (2019), 1804726.
- [56] C. Li, C. Koenigsmann, W. Ding, B. Rudshteyn, K.R. Yang, K.P. Regan, S.J. Konezny, V.S. Batista, G.W. Brudvig, C.A. Schmuttenmaer, Facet-dependent photoelectrochemical performance of TiO2 nanostructures: an experimental and computational study. J. Am. Chem. Soc. 137 (2015) 1520–1529.
- [57] J. Pan, G. Liu, G.Q. Lu, H.M. Cheng, On the true photoreactivity order of {001,010}, and {101} facets of anatase TiO2 crystals, Angew. Chem. Int. Ed. 50 (2011) 2133–2137.
- [58] T. Wei, Y. Zhu, Y. Wu, X. An, L.-M. Liu, Effect of single-atom cocatalysts on the activity of faceted TiO2 photocatalysts, Langmuir 35 (2018) 391–397.
- [59] T. Tong, B. Zhu, C. Jiang, B. Cheng, J. Yu, Mechanistic insight into the enhanced photocatalytic activity of single-atom Pt, Pd or Au-embedded g-C3N4, Appl. Surf. Sci. 433 (2018) 1175–1183.
- [60] H. Luo, Y. Liu, S.D. Dimitrov, L. Steier, S. Guo, X. Li, J. Feng, F. Xie, Y. Fang, A. Sapelkin, Pt single-atoms supported on nitrogen-doped carbon dots for highly efficient photocatalytic hydrogen generation, J. Mater. Chem. A 8 (2020) 14690–14696.
- [61] S. Meng, J. Zhang, S. Chen, S. Zhang, W. Huang, Perspective on construction of heterojunction photocatalysts and the complete utilization of photogenerated charge carriers, Appl. Surf. Sci. 476 (2019) 982–992.
- [62] G.N. Vayssilov, Y. Lykhach, A. Migani, T. Staudt, G.P. Petrova, N. Tsud, T. Skála, A. Bruix, F. Illas, K.C. Prince, Support nanostructure boosts oxygen transfer to catalytically active platinum nanoparticles, Nat. Mater. 10 (2011) 310–315.
- [63] X. Li, S. Wang, Y. Zhu, G. Yang, P. Zheng, DFT study of bio-oil decomposition mechanism on a Co stepped surface: acetic acid as a model compound, Int. J. Hydrogen Energy 40 (2015) 330–339.